This article has been accepted for publication in a future issue of this journal, but has not been fully edited. Content may change prior to final publication. Citation information: DOI 10.1109/TIP.2016.2592799, IEEE Transactions on Image Processing

Radiometric Compensation of Images Projected on Non-White Surfaces by Exploiting Chromatic Adaptation and Perceptual Anchoring

Tai-Hsiang Huang, Ting-Chun Wang, and Homer H. Chen, *Fellow, IEEE*

***Abstract*—Flat surfaces in our living environment to be used as replacements of a projection screen are not necessarily white. We propose a perceptual radiometric compensation method to counteract the effect of color projection surfaces on image appearance. It reduces color clipping while preserving the hue and brightness of images based on the anchoring property of human visual system. In addition, it considers the effect of chromatic adaptation on perceptual image quality and fixes the color distortion caused by non-white projection surfaces by properly shifting the color of the image pixels toward the complementary color of the projection surface. User ratings show that our method outperforms existing methods in 974 out of 1020 subjective tests.**

***Index Terms*—Radiometric compensation, procam, Vasarely illusion, chromatic adaptation, CIECAM02, Human visual system.**

I. Introduction

UBIQUITOUS projection, meaning being able to project an image anywhere, is no longer a fiction due to the miniaturization of projectors. With an embedded projector, mobile or wearable devices can project an image on any nearby surface such as wall, desktop, floor, clothes, or palm. However, most flat surfaces in our living environment are not conditioned for image projection. Besides geometric deformation, color distortion is inevitably introduced to the projected image. For example, when an image is projected on a wood-top desk, the grain pattern of the wood would blend with the image and affect the image appearance. Similarly, as shown in Fig. 1, when the projection surface is non-white, the color of the surface would affect the image appearance. This work investigates how to combat such color distortion by radiometric compensation.

Manuscript received October 22, 2014. This work was supported in part by a grant from the Ministry of Science and Technology of Taiwan under Contract 103-2221-E-002-119-MY3 and a grant from National Taiwan University under Contract 104R890851.

T.-H Huang is with the Graduate Institute of Communication Engineering, National Taiwan University, Taipei 10617, Taiwan, R.O.C (e-mail: tshuang1983@gmail.com).

T.-C Wang is with the Department of Electrical Engineering, National Taiwan University, Taipei 10617, Taiwan, R.O.C (e-mail: tcwang0509@gmail.com).

H. H. Chen is with the Department of Electrical Engineering, Graduate Institute of Communication Engineering, and Graduate Institute of Networking and Multimedia, National Taiwan University, Taipei 10617, Taiwan, R.O.C (e-mail: homer@ntu.edu.tw).

(a) (b)

Fig. 1. Color blending is inevitable for a non-white projection surface. Appearance of an image projected on (a) a white projection surface and (b) a blue projection surface.

Radiometric compensation can be realized by adding a digital camera to the projector as a visual feedback. The resulting system is called procam, which works by first projecting one or a sequence of calibration patterns to the projection surface. The calibration images captured by the camera are analyzed to identify the characteristics of the projection surface. Then the image to be displayed is compensated accordingly to counteract the effect of a non-white projection surface on image appearance.

In practice, the image, the projector, the camera, and the projection surface all have limited dynamic range and gamut. Furthermore, the dynamic ranges and gamuts of the components of a procam may not be compatible with each other. Such limitations and incompatibility affect the performance of a procam. For example, when the color of the compensated image extends beyond the projector's gamut, color clipping is bound to occur. How to overcome such limitations for radiometric compensation and preserve the perceptual appearance of an image is an important issue.

Besides the physical properties of a color signal, the perceptual properties of human visual system (HVS) have to be considered to bridge the gap between machine perception and human vision [35]. Most radiometric compensation methods assume that two physically different color signals would appear different. This assumption, however, is not necessarily true. It is well known that, due to the chromatic adaptation property of HVS, an object that gives the sensation of white under daylight still appears white under an incandescent light, although the daylight is bluer than the incandescent light.

The fact that our eyes automatically adapt to the display environment unfortunately has a flip side for the problem

This article has been accepted for publication in a future issue of this journal, but has not been fully edited. Content may change prior to final publication. Citation information: DOI 10.1109/TIP.2016.2592799, IEEE Transactions on Image Processing

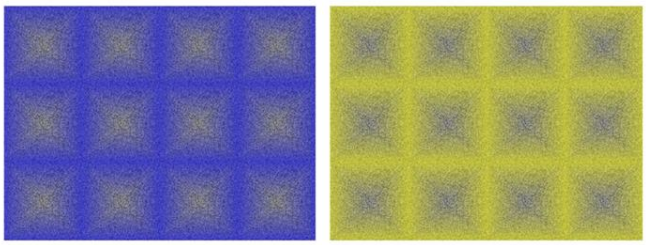

(a) (b)

Fig. 2. Illustration of the chromatic Vasarely illusion. A repeated gray cross-shaped pattern is surrounded by a uniform background of a different color. The cross-shaped pattern illusorily appears to be yellow in (a) and blue in (b) [22].

considered here in that a color would appear differently when it is surrounded by a different color background. This perceptual property of HVS can be best illustrated by the chromatic Vasarely illusion [22]. Only gray and blue colors are used to generate the pattern shown in Fig. 2(a). But the HVS is tricked into seeing yellow (the complementary color of blue) in the gray crosses because the blue background affects the color perception of HVS. Similarly, the gray cross-shaped pattern in Fig. 2(b) illusorily appears to be blue in a yellow background. For non-white projection surfaces, it is important to address the effect of color background on image appearance.

This paper is different from our previous work [32] in that the projection surfaces are not limited to be uniform color. Our system can deal with texture surfaces now (Section III), and we include an analysis of computational efficiency, accuracy, and optimization in Section V.

The contributions of the paper are as follows:

- We propose an optimization method for radiometric compensation to reduce the clipping artifact while preserving the photometric (lightness, hue, and chroma) quality of the image. All parameters of the method are determined through subjective tests to ensure that the design is in conformance with human visual perception (Section III).
- Unlike most existing radiometric compensation methods, our method considers the effect of chromatic adaptation on ubiquitous projection and yields more faithful color reproduction (Section III).
- We simplify the nonlinear color transformations of CIECAM02 [16] and reduce the computation time by 50% with only 2.3% approximation error (Section IV). The speedup is important for practical applications.

II. Review

This section briefly reviews the radiometric compensation techniques, the chromatic adaptation property of HVS, the anchoring theory, the CIECAM02 model, and the color clipping reduction techniques.

A. Radiometric Compensation

The procam model developed by Grossberg *et al*. [1] has been widely adopted to describe the color conversion process of a procam and relate the input intensity of the projector all the way to the output intensity of the camera. A calibration procedure is required to determine the projector response function, the surface reflectance function, and the camera response function for the procam model. The first two are often combined into a new function $P(\cdot)$ that relates the input intensity of the projector to the output irradiance of the projection surface. The calibration for the ideal white surface and the color projection surface are performed separately.

Given $P(\cdot)$, the radiometric compensation works by first computing the irradiance R of an input image on the white screen from the image intensity I,

$$R = P_W(I), \tag{1}$$

where the subscript W denotes a white screen. Then the image is compensated such that the irradiance of the compensated image on the color projection surface is equal to that of the image on the white screen. That is,

$$P_C(I') = P_W(I), \tag{2}$$

where the subscript C denotes a color projection surface and I' denotes the compensated image. Taking the inverse conversion on both sides of (2) yields

$$I' = P_C^{-1}(P_W(I)). \tag{3}$$

The above procedure works under the ideal condition with no limitation on the dynamic range and gamut of each procam component. We take such limitation into consideration in Section III.

Grossberg's model [1] cannot accurately describe the non-linearity of color mixing [1] between the projector and the camera. A more accurate model was developed by Grundhöfer [34].

B. Anchoring Theory

The anchoring theory of lightness perception suggests that HVS tends to first identify the highest luminance of an image as the anchor and then determine the appearance of the image with respect to the anchor [14]. In the context of color perception, the anchor refers to a set of tristimulus values or chromaticity coordinates that define the "white" color of the image.

Anchoring is a perceptual tendency that accounts for the chromatic adaptation property of HVS. Take Fig. 2(a) as an example. When looking at the cross-shaped pattern, our eyes take a slightly blue color as white because blue has the highest dominant brightness in the image. As a result, the appearance of the image would bias slightly toward the complementary color of blue, which is yellow. This is why the gray cross-shaped pattern appears yellowish in Fig. 2(a). Likewise, the gray cross-shaped pattern in Fig. 2(b) appears bluish because our visual perception of the pattern is slightly shifted toward the complementary color of yellow, which is blue.

C. CIECAM02 Color Appearance Model

CIECAM02 is the most recent color appearance model ratified by the CIE Technical Committee [16]. It provides a mathematical description of the relationship between the

This article has been accepted for publication in a future issue of this journal, but has not been fully edited. Content may change prior to final publication. Citation information: DOI 10.1109/TIP.2016.2592799, IEEE Transactions on Image Processing

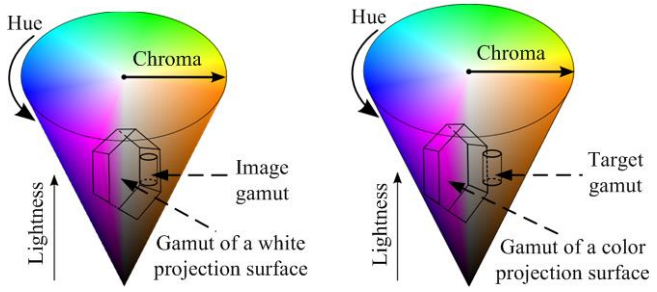

Fig. 3. Explanation of color clipping by the spatial relation between the image gamut and the projection surface gamut in a 3D color space. (a) Since the gamut of the image lies completely within the gamut of the ideal white projection surface, there is no color clipping. (b) When the target gamut is not entirely enclosed by the gamut of the color projection surface, color clipping is bound to happen.

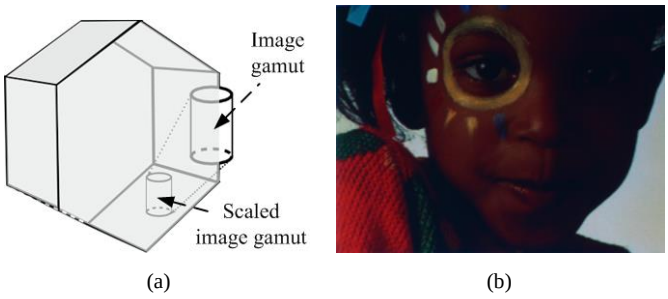

Fig. 4. (a) Illustration of how image gamut scaling can reduce the color clipping artifact in a 3D color space. The spatial relation between the image gamut and the projection surface gamut is adopted from Fig. 3(b). The image gamut is scaled down to within the projection surface gamut to avoid color clipping. (b) A compensated image thus obtained.

physically measurable quantities of stimuli and the attributes of visual sensation. Specifically, it relates the CIE tristimulus values [15] to six attributes of visual sensation: brightness, lightness, colorfulness, chroma, hue, and saturation.

CIECAM02 requires a user-specified reference white as the anchor for computing the appearance of an input color with respect to the reference white. The degree of chromatic adaptation is controlled by a parameter *D* ranging from 0 for no adaptation to 1 for complete adaptation. The model can be implemented in forward or backward manner. In the forward manner, the model outputs the appearance attributes of a color with respect to a given reference white. In the backward manner, the model generates a color using the input appearance attributes and the reference white. All the image operations described in Section III are based on CIECAM02. We adopt this color appearance model in our method because of its accuracy and flexibility [33]. It has the following advantages over CIELAB and CIELUV:

- Viewing condition parameters can be set to represent the display's viewing conditions.
- Reference white can be changed over a wide range reliably.
- They provide more numerical correlates for all perceived attributes of color (colorfulness, chroma, saturation, hue, brightness, and lightness)
- Numerical scales of these correlates correspond better to color perception than CIELUV correlates.
- CIECAM02 is a more uniform color space for small and large color differences.

D. Color Clipping Artifact

Whether the image color can be properly displayed on a projection surface has to do with the gamut of the image with respect to the gamut of the projection surface. If the image gamut is not entirely inside the gamut of the projection surface, color clipping would occur and result in noticeable artifact. This is illustrated in Fig. 3. For ubiquitous projection, the gamut of the image on an ideal white screen serves as the target gamut, which often falls outside or across the gamut of the projection surface. To reproduce the appearance of an image on a color projection surface with as little color clipping as possible, the image gamut has to be properly manipulated with respect to the gamut of the projection surface.

The methods for reducing color clipping artifact can be divided into the multi-projector approach [2]–[4] and the single-projector approach [5]–[13]. The former expands the gamut of the projection surface by superimposing the images projected from a number of projectors; color clipping artifact is reduced at the expense of system complexity and cost. The latter involves a scaling operation that shrinks the image gamut, as shown in Fig. 4(a), at the expense of image brightness and details. In general, artifact is introduced as a result of improper scaling.

Both heuristic and perceptual metrics can be used to quantify the effect of color clipping and dimming on image quality. For example, root-mean-square error has been adopted to measure radiometric distortion [23], and a perception-based error metric [24] that considers contrast sensitivity [25] and visual masking [26] of HVS has been used to measure the noticeable luminance distortion [7]. Generally, the quality of error metric affects the performance of a radiometric compensation method.

III. Proposed Method

Conventional radiometric compensation attempts to completely reproduce the color tone of an image. However, due to the physical limitation on the gamut of a projector, the brightness and color tone usually cannot be perfectly recovered at the same time by radiometric compensation. Therefore, a tradeoff between brightness and color tone has to be made.

Fig. 5 illustrates how the conventional method works for a single pixel in the linear RGB color space. Suppose the color of the projection surface is magenta and the target color is X_0. When X_0 is projected onto the magenta surface, the complementary color of magenta—which is green—would be partially absorbed by the projection surface, and the reflected color would be biased toward magenta. To compensate for the absorption of the green color, the conventional method increases the intensity of the green channel from X_0 to X_1 so that, when projecting X_1 onto the projection surface, the reflected color would be exactly X_0. However, in practice, this reflected color would appear greener than X_0 due to the chromatic adaptation of HVS.

This article has been accepted for publication in a future issue of this journal, but has not been fully edited. Content may change prior to final publication. Citation information: DOI 10.1109/TIP.2016.2592799, IEEE Transactions on Image Processing

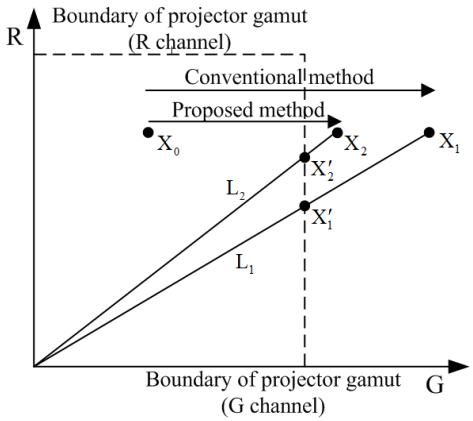

Fig. 5. The difference between the proposed method and the conventional method in radiometric compensation.

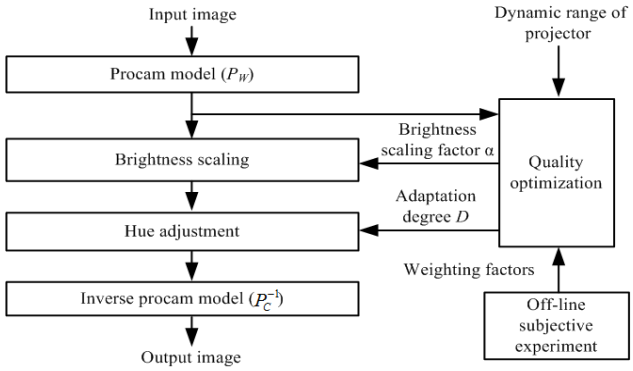

Fig. 6. Block diagram of the proposed algorithm.

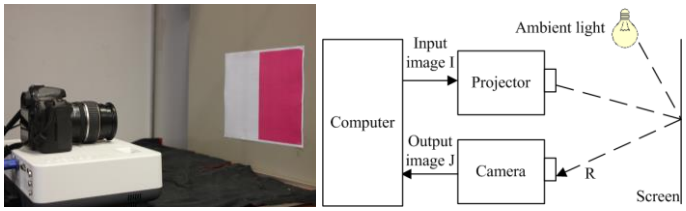

(a) (b)

Fig. 7. (a) Experimental setup. The procam system consists of a projector (SANYO PLC-XW56) and a camera (Canon 40D). (b) The architecture of procam system.

To compensate for the chromatic adaptation, we adjust the projected color from X_1 to a less green color X_2. It should be noted that X_0, X_1, and X_2 would be collinear in most real cases because the compensation for the projection surface color and the compensation for the chromatic adaption are both based on the color of the projection surface. The only difference between them is that the former increases while the later decreases the intensity of the green channel of X_0. Because the amount of color adjustment due to chromatic adaptation is smaller than that due to surface color compensation, X_2 would lay between X_0 and X_1.

The projected color may not lay inside the projector gamut. Like the conventional method, our proposed method solves the problem by scaling down the projected color along the line passing through the origin to preserve the hue of the color at the cost of brightness (the distance from a color to the origin). However, the proposed method results in brighter image than the conventional method. This is illustrated in Fig. 5, where X_1' and X_2', respectively, are the scaled colors generated by the conventional and the proposed methods. Since L_2 (the distance between X_2' and the origin) is larger than L_1 (the distance between X_1' and the origin), the image generated by the proposed method is brighter than that generated by the conventional method.

When the color of the background surface under white illumination is not visible at all, the amount of hue adjustment would be very small because the target background color is nearly black. For such cases, our algorithm would not adjust the color of the image, similar to the conventional radiometric compensation algorithm.

Based on the radiometric compensation procedure described in Section II. A, we propose an optimization method to reduce the color clipping artifact while preserving the color appearance of the compensated image as much as possible. The block diagram of the proposed method is shown in Fig. 6. First, we adopt Grossberg's procam model [1] described in Section II.A to compute the irradiance of an image projected on a white surface via $P_W(\cdot)$. Then, a brightness scaling and a hue adjustment operation are applied to the image with optimized coefficients. Finally, we perform radiometric compensation via $P_C^{-1}(\cdot)$. The details of our method are described as follows.

A. Calibration of the Procam Model

The procam system considered in this work consists of a projector (SANYO PLC-XW56) and a camera (Canon 40D). The experimental setup and the corresponding block diagram are shown in Fig. 7.

The irradiance R of a pixel located at (x, y) of a projected image can be modeled by

$$\begin{aligned} R(x,y) &= P(I(x,y), r(x,y), a(x,y)) \\ &= p(I(x,y)) \cdot r(x,y) + a(x,y) \end{aligned}, \tag{4}$$

where $p(\cdot)$ is the projector response function, $r(x, y)$ is the reflectance of the surface, and $a(x, y)$ is the irradiance contributed by the ambient light. To determine $r(x, y)$ and $a(x, y)$, we project two gray images with different intensity levels I_1 and I_2 onto the projection surface and obtain the corresponding irradiances $R_1(x, y)$ and $R_2(x, y)$, respectively, as follows:

$$\begin{cases} R_1(x,y) = p(I_1) \cdot r(x,y) + a(x,y) \\ R_2(x,y) = p(I_2) \cdot r(x,y) + a(x,y) \end{cases}. \tag{5}$$

Therefore,

$$\begin{cases} r(x,y) = \dfrac{R_1(x,y) - R_2(x,y)}{p(I_1) - p(I_2)} \\ a(x,y) = R_2(x,y) - p(I_2) \cdot \dfrac{R_1(x,y) - R_2(x,y)}{p(I_1) - p(I_2)} \end{cases}. \tag{6}$$

Substituting (6) into (4) yields

$$R(x,y) = R_2(x,y) + \left[p(I(x,y)) - p(I_2) \right] \frac{R_1(x,y) - R_2(x,y)}{p(I_1) - p(I_2)}. \tag{7}$$

This article has been accepted for publication in a future issue of this journal, but has not been fully edited. Content may change prior to final publication. Citation information: DOI 10.1109/TIP.2016.2592799, IEEE Transactions on Image Processing

Rewriting (4) by putting the non-linear terms together and denote them by $N(\cdot)$, we have

$$\begin{aligned} R(x,y) &= R_2(x,y) + \frac{p(I(x,y)) - p(I_1)}{p(I_1) - p(I_2)}\big(R_1(x,y) - R_2(x,y)\big) \\ &= R_2(x,y) + N(I(x,y))\big(R_1(x,y) - R_2(x,y)\big) \end{aligned}. \quad (8)$$

Note that $N(\cdot)$ is independent of the reflectance of the texture surface because it is only related to the input image and the projector's response function. On the other hand, the terms $R_2(x, y)$ and $(R_1(x, y) - R_2(x, y))$ implicitly represent the reflected irradiance of the ambient light and the reflectance of the textured surface at (x, y).

From (8), we have

$$N(I(x,y)) = \frac{R(x,y) - R_2(x,y)}{R_1(x,y) - R_2(x,y)}. \quad (9)$$

Note that since the value of $I(x, y)$ is an integer ranging from 0 to 255, $N(\cdot)$ can theoretically be obtained for all 256 possible inputs. In practice, since there are noises in the obtained irradiance data, $N(\cdot)$ is determined by regression. Specifically, we project a calibration pattern with intensity levels uniformly distributed from 0 to 255 onto the texture surface. From the captured image, we can obtain multiple irradiance values corresponding to each of the 256 possible inputs of $N(\cdot)$. Then $N(\cdot)$ is determined by regression.

B. Color Mixing between Projector and Camera

Grossberg's color decoupling method [1] and its corresponding calibration procedure are adopted in this work to deal with the color mixing [1] between projector and camera. Specifically, the irradiance $\tilde{R}$ captured by the camera is modeled by

$$\tilde{R} = V\tilde{P} + \tilde{a}, \quad (10)$$

where V is a 3-by-3 matrix, $\tilde{P}$ is the irradiance of the projector, and $\tilde{a}$ is the reflected irradiance of the ambient light. $\tilde{R}$, $\tilde{P}$, and $\tilde{a}$ are 3-vectors. Grossberg et al. decompose V into the multiplication of two terms as follows:

$$V = \begin{bmatrix} V_{RR} & V_{RG} & V_{RB} \\ V_{GR} & V_{GG} & V_{GB} \\ V_{BR} & V_{BG} & V_{BB} \end{bmatrix} = \begin{bmatrix} 1 & \tilde{V}_{RG} & \tilde{V}_{RB} \\ \tilde{V}_{GR} & 1 & \tilde{V}_{GB} \\ \tilde{V}_{BR} & \tilde{V}_{BG} & 1 \end{bmatrix} \begin{bmatrix} r_R & 0 & 0 \\ 0 & r_G & 0 \\ 0 & 0 & r_B \end{bmatrix}, \quad (11)$$

Denoting the first term by $\tilde{V}$ and the second term by $\tilde{r}$ yields

$$V = \begin{bmatrix} 1 & \tilde{V}_{RG} & \tilde{V}_{RB} \\ \tilde{V}_{GR} & 1 & \tilde{V}_{GB} \\ \tilde{V}_{BR} & \tilde{V}_{BG} & 1 \end{bmatrix} \begin{bmatrix} r_R & 0 & 0 \\ 0 & r_G & 0 \\ 0 & 0 & r_B \end{bmatrix} = \tilde{V}\,\tilde{r}, \quad (12)$$

where $\tilde{V}$ models the color mixing between projector and camera, and $\tilde{r}$ models the reflectance of the projection surface. Specifically, in (11), each $\tilde{V}_{C_1C_2}$ models the contribution of the C_1 channel of the projector to the C_2 channel of the camera, and r_{C_1} models the reflectance of the projection surface corresponding to the C_1 channel of the projector.

Each $\tilde{V}_{C_1C_2}$ in (11) is determined separately by projecting two images with intensity difference only in the C1 color channel of the projector and normalizing the resulting irradiance difference in each camera channel.

C. Brightness Scaling

We reduce the color clipping artifact by shrinking the image gamut while preserving the image appearance as much as possible. The idea is similar to that illustrated in Fig. 5 except that the operation is performed in the 6D color-appearance space specified by CIECAM02 instead of a 3D color space. A major benefit of CIECAM02 is that it allows us to incorporate the anchoring property of human color perception and preserve the relative attributes of lightness, chroma, and hue of an image across different projection surfaces. In addition, the accuracy of CIECAM02 has been verified by rigorous test procedures [31].

There are two steps. In the first step, the attributes of visual sensation of the image are computed using CIECAM02, for which the reference white is set to the highest luminance of the image. In the second step, the luminance of the reference white is scaled down and used as a reference to transform the visual attributes obtained in the previous step to the color space of the image. Since the color appearance of the image is to be preserved, we do not modify the visual attributes.

The details of brightness scaling are as follows. First, the intensities of the input image are transformed to the luminance values on the white surface using the intensity-to-luminance function $P_W(\cdot)$ described in Section II.A. Then, the luminance values are normalized and transformed to the XYZ tristimulus values. The largest tristimulus value T_W is identified and used as the reference white in the forward transformation of CIECAM02 to relate each tristimulus value to the six visual attributes. Finally, these visual attributes are transformed back to the luminance values with respect to a new white point αT_W, where α is a brightness scaling factor that is determined through a quality optimization process described in Section III.E.

D. Hue Adjustment

The purpose of hue adjustment is to compensate the effect of chromatic adaptation of HVS on the color appearance of an image. An illustration of the effect is shown in Fig. 8, where the background represents a projection surface and the foreground represents an image. The top blue image block is projected on a white surface. The bottom row shows the scenario where the same blue image block is projected on a blue projection surface. The traditional radiometric compensation method would aim for a perfect restoration and generate the bottom left blue image. Apparently, even if the color of the compensated image is physically restored, it appears different from the top blue image block. In contrast, our hue adjustment operation would make the compensated image block shown on the bottom right a little bit bluer, and hence the color appearance of the resulting image would be closer to the top image block.

Similar to the brightness scaling operation, the hue of an image is adjusted by manipulating the color of the reference white of the CIECAM02 model. It involves several steps. First,

This article has been accepted for publication in a future issue of this journal, but has not been fully edited. Content may change prior to final publication. Citation information: DOI 10.1109/TIP.2016.2592799, IEEE Transactions on Image Processing

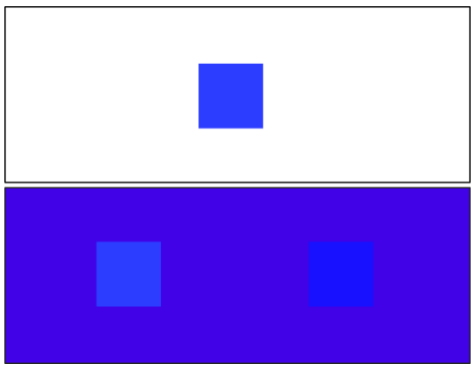

Fig. 8. An illustration of the effect of hue adjustment. The top half shows a blue image block projected on a white surface. The bottom half shows two image blocks projected on a blue surface. The two image blocks are generated from the top image block in two different ways. The left one is physically the same color as the top image block, and the right one is with hue adjustment. It appears that the right image block is perceptually more similar to the top image block than the left one.

(a) (b)

Fig. 9. (a) Setup of the off-line subjective experiment. The left part of the projection area is white and the right part is a color surface. (b) The original test image is projected onto the white projection surface, and the compensated image is projected onto the color projection surface. The subject can switch the image on the color projection surface between two compensated images generated with different w_1 and w_2 in each trial.

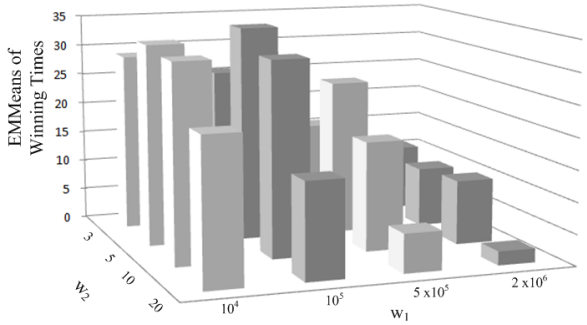

Fig. 10. The EMMeans of the winning times of different combinations of w_1 and w_2.

the visual attributes of the input image are computed using the same procedure for brightness scaling. Next, $P_C(\cdot)$ is applied to the largest intensity of the input image to obtain its luminance on the color surface, which is then normalized and transformed to obtain the tristimulus value $\tilde{T}_W$. Finally, the color appearance of the input image is transformed back using $\tilde{T}_W$ as the white point.

Recall that the degree of chromatic adaptation is controlled in the CIECAM02 model through the chromatic adaptation degree D, which ranges from 0 for no adaptation to 1 for complete adaptation. We use this parameter to control the amount of hue adjustment of a color toward $\tilde{T}_W$. The larger the value of D, the more hue adjustment is performed. Similar to the brightness scaling factor α, D is also determined through a quality optimization process.

E. Quality Optimization

We find the optimal α and D that balance the undesirable brightness reduction, hue distortion, and color clipping in the compensated image through the following optimization procedure:

$$(\alpha, D) = \arg\min_{\alpha, D} \left\{ w_1 \left[(1-\alpha)^2 + w_2 D^2 \right] + E(\alpha, D) \right\}, \quad (13)$$

where (1-α) accounts for the brightness reduction of the resulting image, D accounts for the amount of hue adjustment, and E accounts for the amount of clipping artifact in the compensated image, which is calculated as follows:

$$E(\alpha, D) = \sum_i l\{p_i(\alpha, D) > U\} \left(p_i(\alpha, D) - U \right)^2 / |I|, \quad (14)$$

where l is an indicator function, p_i is the luminance value of pixel i in the compensated image, U is the upper bound of the projector's dynamic range, and $|I|$ denotes the total number of pixels in the image. It should be noted that p_i is a function of α and D because the luminance value of the compensated iamge changes whenever α or D changes.

The weightings w_1 and w_2 are determined through an off-line subjective experiment which aims at making the optimization in conformance with human visual perception. The details are described as follows.

F. Off-Line Subjective Experiment

A subjective test involving 10 male and 10 female subjects was conducted to determine w_1 and w_2 in (13). The age of the subjects ranges from 21 to 26. Since it is infeasible to test the infinitely many possible values of w_1 and w_2, we empirically chose four candidate values (3, 5, 10, and 20) for w_1 and another four values (10^4, 10^5, 5×10^5, and 2×10^6) for w_2 that produce images with better quality (judged subjectively by the authors). In the test, we used 10 test images selected from three image data sets: Waterloo [18], Kodak [19], and SIPI [20]. Each test image was compensated using the (α, D) generated by the 16 combinations of the candidate values of w_1 and w_2. This way, we had 16 compensated images that correspond to the 16 combinations of weights (w_1 ,w_2) for each test image.

The experimental setup is shown in Fig. 9. The task of the subjects was to choose from the 16 compensated images the one that best matches the original image projected on a white surface. The comparison proceeded in a pair-wise manner. Specifically, in each trial, a subject was presented two randomly selected compensated images projected on a color surface along with the original image projected on a white surface. The one that is more similar to the original image was kept, and the other one was substituted with another randomly selected compensated image that has not yet been shown to the subject. This process repeated until all compensated images were tested.

The experiment was performed on magenta, yellow, and blue projection surfaces. We determined one set of weighting coefficients for all color surfaces. An ANOVA [21] of two factors (w_1 and w_2) was conducted on the total number of times each combination won. The estimated marginal means (EMMEANS) are shown in Fig. 10. We can see that the best

This article has been accepted for publication in a future issue of this journal, but has not been fully edited. Content may change prior to final publication. Citation information: DOI 10.1109/TIP.2016.2592799, IEEE Transactions on Image Processing

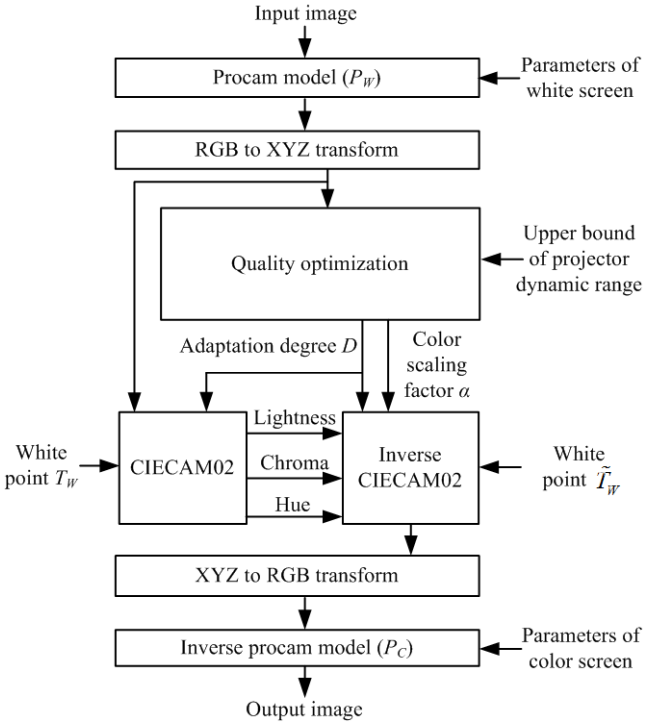

Fig. 11. Block diagram of the proposed algorithm.

performance is achieved when $w_1 = 10^5$ and $w_2 = 5$. This weight combination is adopted in our implementation.

IV. Simplification

The brightness scaling and hue adjustment operations presented in Section III are computationally heavy because of the nonlinear color transformations of CIECAM02.

To reduce the computational cost, two simplifications are proposed: 1) reducing the use of CIECAM02 by combining the brightness scaling and hue adjustment operations, and 2) simplifying the CIECAM02 model. The details of these two simplifications are described in this section.

A. Procedure Simplification

The brightness scaling and hue adjustment are combined into one transformation. In this new transformation, the luminance values of the image are transformed to appearance values using T_W as the white point and then transformed back using $\alpha\tilde{T}_W$ as the white point. The overall block diagram of the simplified procedure is shown in Fig. 11.

B. Model Simplification

The forward and backward transformations of the CIECAM02 model are time consuming due to the non-linear color transformations. Because only the anchor is replaced in the forward and backward transformations, it is possible to simplify the entire process.

CIECAM02 makes use of the CAT02 space [27] for the chromatic adaptation transform and the Hunt-Pointer-Estevez space [28] for computing perceptual attribute correlates. The reader is referred to [16] for the details of CIECAM02. In the following, we use the same notations as those in [16] and only introduce the new notations of the simplified model.

1) Forward transformation: We follow the original model to transform an input color from the CIEXYZ space to the CAT02 space using the M_{CAT02} transformation matrix:

$$\begin{bmatrix} R \\ G \\ B \end{bmatrix} = M_{CAT02}\begin{bmatrix} X \\ Y \\ Z \end{bmatrix} = \begin{bmatrix} 0.7328 & 0.4296 & -0.1624 \\ -0.7036 & 1.6975 & 0.0061 \\ 0.0030 & 0.0136 & 0.9834 \end{bmatrix}\begin{bmatrix} X \\ Y \\ Z \end{bmatrix}. \quad (15)$$

Then, the chromatic adaptation transform for the R channel is approximated by

$$R_c = \left(\frac{Y_w}{R_w}D + 1 - D\right)R \cong (1-D)R, \quad (16)$$

where R_c is the adapted R value of the input color, Y_w and R_w, respectively, are the luminance and R values of the reference white, and D is the degree of adaptation. The same approximation is also applied to obtain G_c and B_c. Then, according to the original model, we transform the adapted color from the CAT02 space to the Hunt–Pointer–Estévez space by the M_H transformation matrix,

$$\begin{bmatrix} R' \\ G' \\ B' \end{bmatrix} = M_H M_{CAT02}^{-1}\begin{bmatrix} R_c \\ G_c \\ B_c \end{bmatrix}. \quad (17)$$

Substituting (15) and (16) into (17) yields

$$\begin{bmatrix} R' \\ G' \\ B' \end{bmatrix} \cong (1-D)M_H\begin{bmatrix} X \\ Y \\ Z \end{bmatrix}. \quad (18)$$

A non-linear response compression based on the generalized Michaelis–Menten equation [29] is then applied to the adapted color. For the R' channel, the compression can be approximated as follows:

$$R'_a = \frac{400(F_L R'/100)^{0.42}}{27.13 + (F_L R'/100)^{0.42}} + 0.1 \cong \frac{400}{27.13}(F_L R'/100)^{0.42}, \quad (19)$$

where F_L is a luminance adaptation factor,

$$F_L = 0.2\left(\frac{1}{5L_A+1}\right)^4(5L_A) + 0.1\left(1-\left(\frac{1}{5L_A+1}\right)^4\right)^2(5L_A)^{\frac{1}{3}}, \quad (20)$$

and L_A is the luminance of the adapting field in cd/m^2 [16]. The same approximation is also applied to G'_a and B'_a. Then the achromatic response A can be approximated as follows:

$$A = \left(2R'_a + G'_a + \frac{1}{20}B'_a - 0.305\right)N_{bb} \cong \left(2R'_a + G'_a + \frac{1}{20}B'_a\right)N_{bb}, \quad (21)$$

where N_{bb} is a temporary quantity [16] determined by

$$N_{bb} = 0.725\left(\frac{Y_b}{Y_w}\right)^{-0.2}, \quad (22)$$

This article has been accepted for publication in a future issue of this journal, but has not been fully edited. Content may change prior to final publication. Citation information: DOI 10.1109/TIP.2016.2592799, IEEE Transactions on Image Processing

and Y_b is the luminance of the background. Finally, the lightness attribute is approximated by

$$J = 100\left(\frac{A}{A_w}\right)^{cz} \cong 100\left(\frac{2R'_a + G'_a + B'_a/20}{2R'_{wa} + G'_{wa} + B'_{wa}/20}\right)^{cz} \tag{23}$$

where A_w is the achromatic response of the reference white, R'_{wa}, B'_{wa}, and G'_{wa} are the adapted color values of the reference white, c is a viewing condition parameter that can be set to 0.525 for dark surround, 0.59 for dim surround, and 0.69 for normal surround, and z is computed by

$$z = 1.48 + \sqrt{\frac{Y_b}{Y_W}}. \tag{24}$$

2) Backward transformation: Let $\tilde{Y}_w$ be the Y component of the new reference white and denote the ratio of $\tilde{Y}_w$ to Y_w by k. Then, we have

$$\tilde{Y}_w = kY_w, \tag{25}$$

Here, all symbols with a tilde on top denote values derived in the backward process, i.e., from the new reference white. The achromatic response $\tilde{A}_w$ of the new white point only needs to be calculated once for the entire image and is exactly calculated. Let the ratio of $\tilde{A}_w / A_w$ be β. From (23), we have

$$A = A_w\left(\frac{J}{100}\right)^{1/cz} \tag{26}$$

Then,

$$\begin{aligned}\tilde{A} &= \tilde{A}_w\left(\frac{J}{100}\right)^{1/c\tilde{z}} = \beta A_w\left(\frac{J}{100}\right)^{1/c\tilde{z}} = \beta\left(A\left(\frac{J}{100}\right)^{-1/cz}\right)\left(\frac{J}{100}\right)^{1/c\tilde{z}}, \\ &= \beta\left(\frac{J}{100}\right)^{1/c\tilde{z}-1/cz} A = \gamma A,\end{aligned} \tag{27}$$

where $\gamma = \beta\left(J/100\right)^{1/c\tilde{z}-1/cz}$. The correlate for yellow-blue $\tilde{b}$ can be calculated by

$$b = \frac{cp_2}{p_1 \csc h + d\cot h + f} \cong \frac{cp_2}{p_1 \csc h},\ \tilde{b} \cong \frac{c\tilde{p}_2}{\tilde{p}_1 \csc h} \cong \frac{\tilde{p}_2}{p_2}\frac{p_1}{\tilde{p}_1} b, \tag{28}$$

where

$$\tilde{p}_1 = \frac{50000}{13} N_c e_t \frac{\tilde{N}_{cb}}{\tilde{t}} = \frac{\tilde{N}_{cb}}{N_{cb}}\frac{t}{\tilde{t}} p_1 = \left(\frac{\tilde{Y}_w}{Y_w}\right)^{0.2}\frac{t}{\tilde{t}} p_1 = k^{0.2}\frac{t}{\tilde{t}} p_1, \tag{29}$$

$$\tilde{p}_2 = \tilde{A}/\tilde{N}_{bb} + 0.305 \cong \frac{\tilde{A}/\tilde{N}_{bb}}{A/N_{bb}} p_2 \cong k^{-0.2}\gamma p_2, \tag{30}$$

and

$$\tilde{t} = \left(\frac{1.64 - 0.29^n}{1.64 - 0.29^{n/k}}\right)^{0.8111} t \cong k^{0.2} t. \tag{31}$$

Thus,

$$\tilde{b} \cong \frac{\tilde{p}_2}{p_2}\frac{p_1}{\tilde{p}_1} b = k^{-0.4}\frac{\tilde{A}}{A}\frac{\tilde{t}}{t} b \cong k^{-0.2}\gamma b, \tag{32}$$

Similarly, the correlate for red-green is

$$\tilde{a} = \tilde{b}\cot h = k^{-0.2}\gamma a, \tag{33}$$

Thus the responses in Hunt–Pointer–Estévez space and its compression are

$$\begin{aligned}\begin{bmatrix}\tilde{R}'_a \\ \tilde{G}'_a \\ \tilde{B}'_a\end{bmatrix} &= \begin{bmatrix}2 & 1 & 1/20 \\ 1 & -12/11 & 1/11 \\ 1/9 & 1/9 & -2/9\end{bmatrix}^{-1}\begin{bmatrix}\tilde{p}_2 \\ \tilde{a} \\ \tilde{b}\end{bmatrix} \\ &\cong k^{-0.2}\gamma\begin{bmatrix}2 & 1 & 1/20 \\ 1 & -12/11 & 1/11 \\ 1/9 & 1/9 & -2/9\end{bmatrix}^{-1}\begin{bmatrix}p_2 \\ a \\ b\end{bmatrix} \cong k^{-0.2}\gamma\begin{bmatrix}R'_a \\ G'_a \\ B'_a\end{bmatrix},\end{aligned} \tag{34}$$

$$\begin{aligned}\tilde{R}' &= \left(\frac{-27\left(\tilde{R}'_a - 0.1\right)}{\tilde{R}'_a - 400.1}\right)^{\frac{1}{0.42}}\frac{100}{F_L} \cong \left(\frac{-27\tilde{R}'_a}{400.1}\right)^{\frac{1}{0.42}}\frac{100}{F_L} \\ &\cong \left(\frac{\tilde{R}'_a}{R'_a}\right)^{\frac{1}{0.42}} R' \cong \left(k^{-0.2}\gamma\right)^{\frac{1}{0.42}} R'.\end{aligned} \tag{35}$$

Finally, the new tristimulus values can be approximated by

$$\begin{bmatrix}\tilde{R}_c \\ \tilde{G}_c \\ \tilde{B}_c\end{bmatrix} \cong M_{CAT02} M_H^{-1}\begin{bmatrix}\tilde{R}' \\ \tilde{G}' \\ \tilde{B}'\end{bmatrix} \cong \left(k^{-0.2}\gamma\right)^{1/0.42}\begin{bmatrix}R_c \\ G_c \\ B_c\end{bmatrix}, \tag{36}$$

$$\tilde{R} = \tilde{R}_c / \left(\frac{Y_w D}{\tilde{R}_w} + 1 - D\right) \cong \left(k^{-0.2}\gamma\right)^{\frac{1}{0.42}}\frac{100D/R_w + 1 - D}{100D/\tilde{R}_w + 1 - D} R. \tag{37}$$

V. EXPERIMENTS

Four experiments were conducted to evaluate the performance of the proposed method. In the first experiment, we evaluated the accuracy and time complexity of the simplified CIECAM02. In the second experiment, we evaluated the effect of hue adjustment on image brightness. In the third experiment, we evaluated the brightness gain of the proposed method. Finally, we performed a subjective experiment to compare our method with four other methods.

A. Accuracy and Time Complexity of the Simplified CIECAM02

We compared the efficiency of CIECAM02 with that of the simplified model by testing them on 1000 normalized luminance values which range from [0.1, 0.1, 0.1] to [1, 1, 1] with step size equals 0.1. For each luminance value, the computation time of each model for performing a forward and a backward color transform was measured. Both models were implemented using MATLAB R2012a on a ThinkPad T430 notebook computer with Intel i5 processor (2.6GHz) and 4GB memory. The average computation time for CIECAM02 is 2.59 × 10^{-4} seconds, while the average computation time for the simplified model is 1.31 × 10^{-4} seconds. The results show that the simplified model reduces about 50% of the computation

This article has been accepted for publication in a future issue of this journal, but has not been fully edited. Content may change prior to final publication. Citation information: DOI 10.1109/TIP.2016.2592799, IEEE Transactions on Image Processing

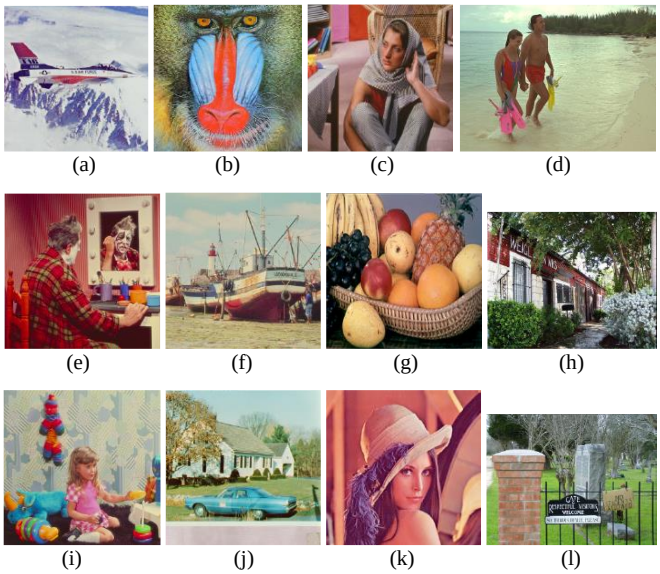

Fig. 12. A set of 12 samples of the 44 test images used in this work.

TABLE I
TIME COMPLEXITY EVALUATION (IN SECONDS)

Image name	Original method	Simplified method	Image name	Original method	Simplified method
avian	18.60	4.08	house3	19.38	3.66
baboon	20.98	4.08	isabe	21.97	4.15
barbara	19.82	4.42	lena	18.35	4.13
beach	18.52	3.68	lighthouse1	18.54	4.32
bikes	14.87	3.82	lighthouse2	17.91	3.57
boats	19.94	4.43	monarch	18.38	4.16
building1	16.60	3.57	ocean	18.09	3.55
building2	17.52	3.54	parrots	17.68	3.45
caps	15.56	3.60	pepper	27.78	4.13
cemetry	17.84	3.81	plane	22.78	4.50
church	18.15	4.03	rapids	18.80	3.78
clown	19.94	4.10	sailing1	18.48	3.94
coins	17.67	3.73	sailing2	18.53	4.34
dancers	18.88	3.80	sailing3	18.87	3.78
dolls	20.49	3.76	sailing4	18.47	3.90
door	17.60	3.45	sculpture	17.51	3.72
fishing	20.76	3.62	statue	17.88	3.63
flower	18.49	3.53	stream	17.56	3.41
fruit	22.01	3.89	wall	21.65	4.17
girl	17.47	4.02	windows	21.03	4.05
house1	17.78	3.72	woman	19.00	3.63
house2	18.81	4.07	womanhat	16.47	3.55

*Original method: 19.22 ± 2.83 (average and standard deviation)
*Simplified method: 3.92 ± 0.46 (average and standard deviation)

time for color transformation.

To investigate the accuracy of the simplified model, we tested it on the same normalized luminance values described above. For each luminance value, a corresponding luminance value was computed using α = 0.1 and D = 0.02. Comparing to the exact solutions computed using CIECAM02, the errors for different luminance combinations are all within ±2.3%, which indicates that the simplified model is accurate enough for color transformation.

We compared the computation time of the original method with that of the simplified method. Both methods were applied to 44 test images (Fig. 12) selected from the image sets of Waterloo [18], Kodak [19], and SIPI [20] but different from the images used in the off-line subjective experiment (Section III.F).

TABLE II
AVERAGE COMPUTATION TIME FOR EACH STEP OF THE PROPOSED METHOD

Main steps	Sub steps	MATLAB codes	C codes
Procam model		0.012s	0.0005s
Quality optimization		3.052s	0.144s*
	Iterations to convergence	120	120
	Cost function of Equation (13)	0.025s	0.0012s
	Equation (14)	0.025s	0.0012s
Brightness scaling + Hue adjustment		0.013	0.0007
Inverse procam model		0.843s	0.041s
Overall computation time		3.92s	0.186s

* Suppose the same solver as our MATLAB implementation is used, the average computation time for the quality optimization would be 0.144s (0.0012s ×120 iterations)

The resulting computation time of each test image is listed in Table I. The average computation time of the original method and the simplified method, respectively, are 19.22 and 3.92 seconds. Approximately 80% of the computation time is saved. In addition, the standard deviation of the computation time is reduced from 2.83 to 0.46.

The average computation time of each step of our MATLAB implementation is shown in Table II. The overall computation time is 3.92s in average, and the quality optimization step, which takes 3.052s, is the main bottleneck.

The overall computation time reduces to 0.186s for the C implementation of the simplified method, as shown in Table II. The computation time is proportional to the number of iterations required for the solver to converge. We take a close look at the bottleneck and find that, in average, 120 iterations are required to obtain the optimal solution.

B. Effect of Hue Adjustment on Image Brightness

The effect of hue adjustment on image brightness was quantitatively evaluated. We forced D, the amount of hue adjustment, to be constant in the optimization process described by (13) and compared the resulting α values across four different levels of hue adjustments: D is set to 0, 0.02, 0.05, and 0.08. A larger α value indicates a brighter image.

A total of 144 uniform color images were used in this evaluation. The hue value ranges from 10 to 360 with a step size of 10, and the chroma value ranges from 25 to 100 with a step size of 25. The test projection surfaces were magenta (hue value is 320), yellow (hue value is 60), and cyan (hue value is 170).

The results for the magenta projection surface are shown in Fig. 13. It can be seen that α varies with respect to the hue and chroma of the test image. It becomes larger when the hue of the test image is closer to the hue of the projection surface, and the peak-to-valley difference increases as the chroma of the test image increases. This reveals how our method adjusts the brightness of a test image based on the color of the projection surface. Fig. 13 also shows that α increases as D increases. This indicates that the larger the hue adjustment, the brighter the resulting image is. Similar observation can be found from the results for the yellow and cyan projection surfaces.

To examine the brightness gain of the hue adjustment, we computed the ratio between α values for trials with hue

This article has been accepted for publication in a future issue of this journal, but has not been fully edited. Content may change prior to final publication. Citation information: DOI 10.1109/TIP.2016.2592799, IEEE Transactions on Image Processing

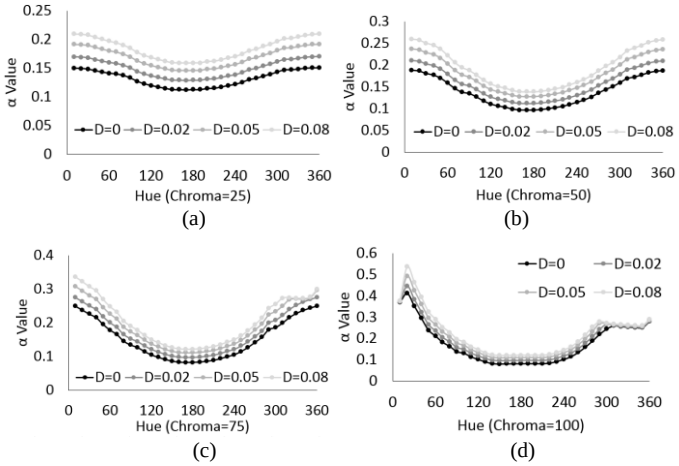

Fig. 13. The α values (color scaling ratio) of uniform color images on a magenta screen (hue value is 320).

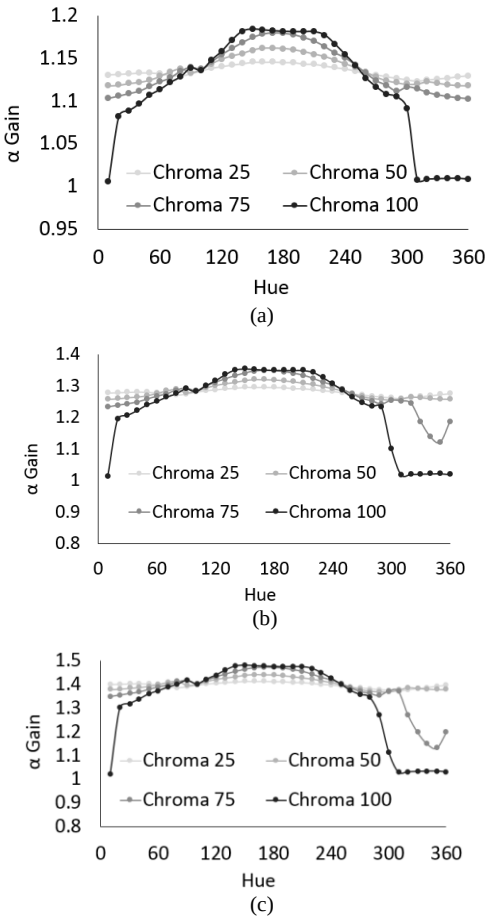

Fig. 14. The α gains (brightness gains) of different test images for a magenta projection surface. (a) Uniform color images with D=0.02, (b) Uniform color images with D=0.05, and (c) Uniform color images with D=0.08.

TABLE III
AVERAGE COLOR SHIFT DUE TO PERCEPTUAL COMPENSATION

D = 0.02	D = 0.05	D = 0.08
6.26%	7.16%	7.42%

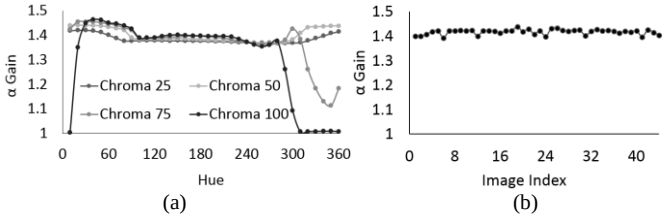

Fig. 15. The α gains (brightness gains) of different test images for a magenta projection surface. (a) Uniform color images and (b) 44 test images.

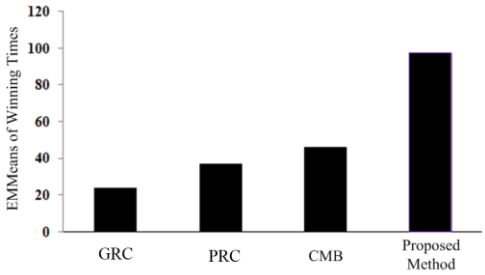

Fig. 16. The EMMeans of the winning times of different algorithms.

adjustment (D = 0.02, 0.05, and 0.08) and without hue adjustment (D = 0). The results for the magenta projection surface are shown in Figs. 14(a)–(c). It can be seen that the α gain increases when the hue of the image is away from magenta, and it reaches the peak value when the hue of the test image is about 160, which is the complementary color of magenta. This indicates that the brightness gain peaks when the hue of the test image is the complementary color of the projection surface.

Finally, we evaluated the percentage of color shift caused by hue adjustment. For each of the 144 uniform color images, we compared between the compensated colors with hue adjustment (D = 0.02, 0.05, and 0.08) and those without hue adjustment (D = 0). The average color shift for each D value is shown in Table III. The amount of color shift increases as D increases, but not in a linear manner. The increment decreases as D increases.

C. Brightness Gain

The brightness gain of the proposed method was evaluated. The 144 uniform color images described in Section V. B and the 44 images described in Table I were used as test images. For each test image, we computed the ratio between the α values with hue adjustment (D and α were obtained by (13)) and those without hue adjustment (D = 0 as described in Section III. B).

Fig. 15(a) shows the results of the uniform color images, where the values of α gain remain nearly constant when the hue of the image is away from the hue of the projection surface. This indicates that the optimization tends to find a D value that maximizes the α gain while preserving the brightness of the colors that are similar to the projection surface. Fig. 15(b) shows the results of the 44 test images. The values of α gain ranges from 1.35 to 1.45, and the average is 1.41.

D. Performance Comparison

To benchmark our method with previous ones, a subjective test was conducted on 34 test images that were not used in the

This article has been accepted for publication in a future issue of this journal, but has not been fully edited. Content may change prior to final publication. Citation information: DOI 10.1109/TIP.2016.2592799, IEEE Transactions on Image Processing

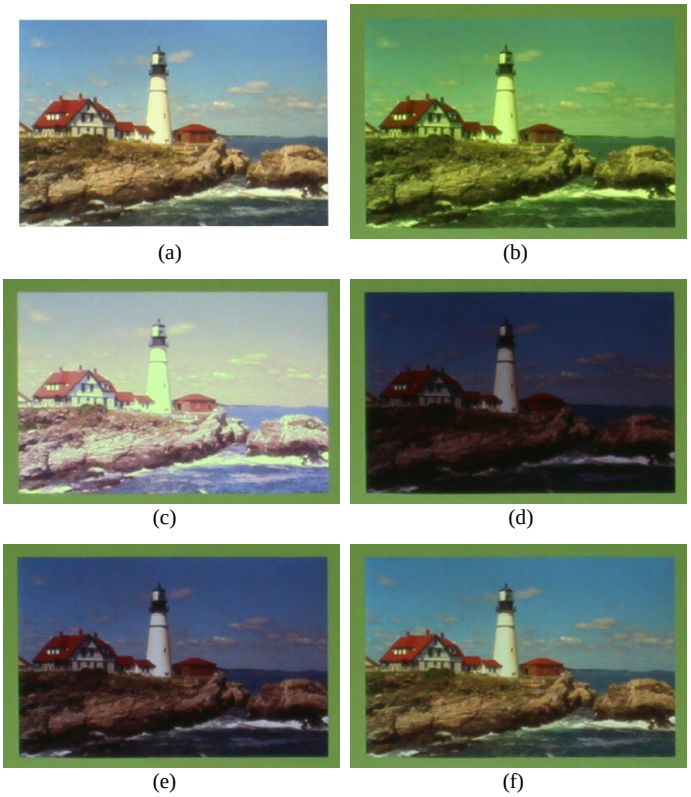

Fig. 17. Comparison of different compensation algorithms. (a) Original image projected on a white screen, (b) Original image projected on a green screen. (c), (d), (e), and (f), respectively, are the compensation results generated by GRC, PRC, CMB, and the proposed methods.

off-line subjective experiment (Section III.D). Five male and five female subjects were involved in the experiment. The age of the subjects ranges from 21 to 26. The proposed method was compared with three other methods: GRC [1], PRC [7], and CMB [13]. We implemented GRC and PRC ourselves and used the original code of CMB.

The procedure was the same as that of the experiment described in Section III.F except that we compared the results for each test image. The results show that the proposed method outperforms the other methods in 974 out of 1020 comparisons (34 test images × 10 subjects × 3 competing algorithms). The wining rate is more than 95%. An ANOVA [21] was conducted on the total number of times each combination won. The EMMEANS of the ANOVA are shown in Fig. 16. The difference in EMMEANS between the proposed method and each of the other methods passes a t-test [38] with a confidence level of 99%, suggesting that the results are statistically reliable.

Figs. 17–19, respectively, show the results of three test images projected on a green, blue, and red projection surface. All the compensation results are captured using a Canon 700D camera with fixed ISO, aperture, and shutter speed. To faithfully present the results, a slightly larger area than the projected image is cropped and shown in the figures so that the readers can see the color and texture of the projection surface.

By examining the coast in Fig. 17, the white house in Fig. 18, the magenta flowers in Fig. 19, we can see that the proposed method preserves image color better than the other methods. In

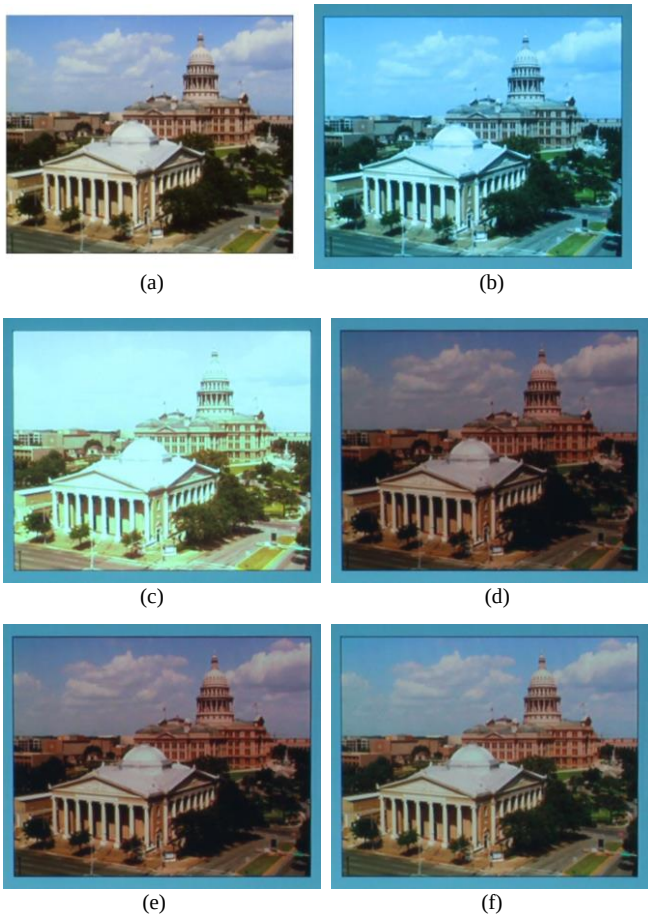

Fig. 18. Comparison of different compensation algorithms. (a) Original image projected on a white screen, (b) Original image projected on a blue screen. (c), (d), (e), and (f), respectively, are the compensation results generated by GRC, PRC, CMB, and the proposed methods.

addition, the proposed method preserves image brightness better than PRC and CMB. This leads to a resulting image with more vivid color (e.g. the yellow color in Fig. 19) and more image details (e.g. the lower part of the coast in Fig. 17 and the tree in Fig. 18). Similar findings about the strength of our algorithm can also be obtained for other test images not shown here.

The results presented above also show the robustness of the proposed algorithm across different color projection surfaces. Since the proposed method has a consistent performance for the red, green, and blue projection surfaces, it would have a similar performance for projection surfaces whose color is a mixture of the primary colors.

The proposed method was compared with three other methods: GRC [1], RRC [36], and PRC [7]. Fig. 20 shows the results of a test image projected on a wood-grain projection surface. Clearly, the results show that the proposed method is better than the other methods in dealing with texture surfaces and that the application of the proposed method is not limited to projection surfaces with uniform color.

VI. LIMITATIONS

Theoretically, not all colors are reproducible because a color

This article has been accepted for publication in a future issue of this journal, but has not been fully edited. Content may change prior to final publication. Citation information: DOI 10.1109/TIP.2016.2592799, IEEE Transactions on Image Processing

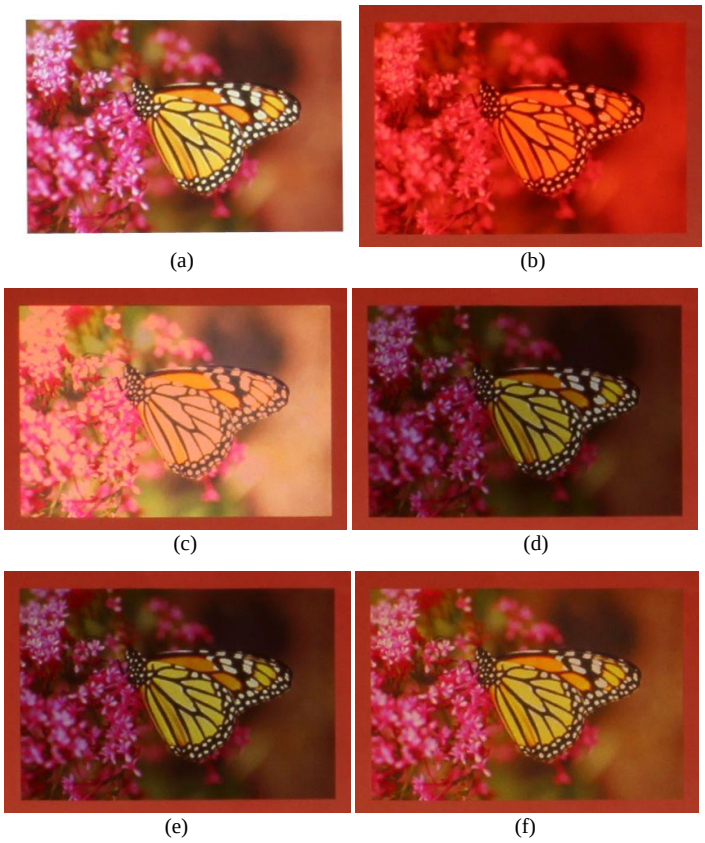

Fig. 19. Comparison of different compensation algorithms. (a) Original image projected on a white screen, (b) Original image projected on a red screen. (c), (d), (e), and (f), respectively, are the compensation results generated by GRC, PRC, CMB, and the proposed methods.

projection surface has a smaller gamut than a white surface. This should be easy to understand by considering the extreme case where a black surface absorbs all wavelengths of the visible light and reflects none. Though gamut mapping can help preserve the color appearance of an image, the color of the image inevitably degrades due to the small gamut of the projection surface.

In practice, the performance of the proposed approach is limited by the resolution of the camera and projector. The camera digitally samples the image shown on the projection surface. The size of each sampled area depends on the camera sensor resolution and the distance of the camera to the projection surface. According to the Nyquist-Shannon sampling theory, an image can be reconstructed from the sampled data if the highest spatial frequency of the image is no greater than one half of the sampling rate. The resolution of the camera automatically imposes an upper bound on the spatial frequency of the image that can be compensated, and so does the projector resolution.

The contrast adaptation of HVS is not considered in this work. Specifically, color appearance depends on adaptation processes of HVS that adjust color sensitivity both to the average of color (through chromatic adaptation) and to the variation of color (through contrast adaptation) [37]. Under complete chromatic adaptation, the average color appears achromatic, and the contrast adaptation alters the perceived color contrast relative to the average color [37]. The chromatic adaptation is modeled in

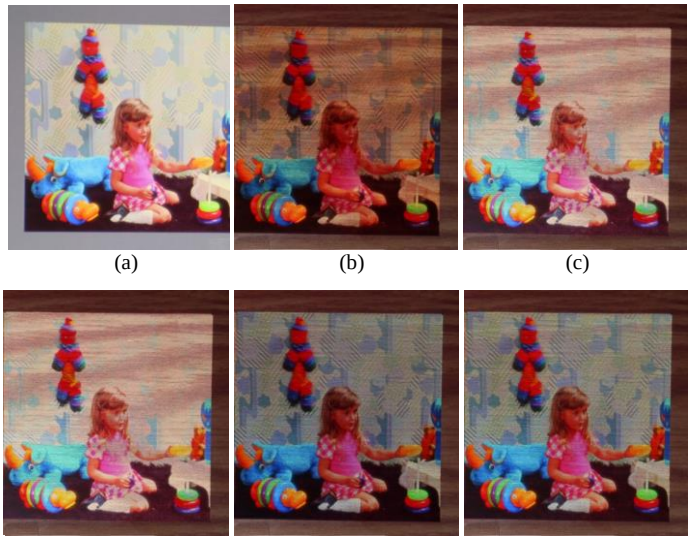

Fig. 20. Comparison of different compensation algorithms. (a) Original image projected on a white screen, (b) Original image projected on a wood-grain surface. (c), (d), (e), and (f) respectively, are the compensation results generated by GRC, RRC, PRC, and the proposed methods.

the proposed method, but the contrast adaptation is not. It would be a topic for future research to investigate how contrast adaptation can be considered in radiometric compensation.

VII. Conclusion

In this paper, we have described a method to improve the radiometric compensation for a procam system. This method adjusts image color based on the anchoring theory to reduce the clipping artifact while preserving the color appearance of the projected image [39]. The proposed method has three notable features. First, it combats the chromatic illusion due to the projection surface by considering the chromatic adaptation property of HVS. Second, unlike previous methods that use a linear approach for brightness scaling, it considers the nonlinear characteristic of human eyes by adopting the CIECAM02 model for all image operations to preserve the image appearance. Finally, the weighting parameters used in the method are determined through a subjective experiment to strike a balance between color clipping and image dimming. As evidenced by user ratings, the proposed method significantly improves the perceptual quality of the compensated images.

References

[1] M. D. Grossberg, H. Peri, S. K. Nayar, and P. N. Belhumeur, "Making one object look like another: controlling appearance using a projector-camera system," in *Proc. IEEE Int. Conf. Computer Vision and Pattern Recognition*, vol. 1, pp. 452–459, Jan. 2004.

[2] A. Majumder and R. Stevens, "LAM: Luminance attenuation map for photometric uniformity in projection based displays," in *Proc. ACM Symp. Virtual Reality Software and Technology*, pp. 147–154, 2002.

[3] A. Majumder, D. Jones, M. McCrory, M. E. Papka, and R. Stevens, "Using a camera to capture and correct spatial photometric variation in multi-projector displays," presented at the *IEEE Int. Workshop on Projector-Camera Systems*, 2003.

[4] D. G. Aliaga, Y. H. Yeung, A. Law, B. Sajadi, and A. Majumder, "Fast high-resolution appearance editing using superimposed projections," *ACM Trans. Graphics*, vol. 31, no. 2, article no. 13, pp. 1–12, Apr. 2012.

[5] O. Bimber, A. Emmerling, and T. Klemmer, "Embedded entertainment with smart projectors," *Computer*, vol. 38, no. 1, pp. 48─55, 2005.

[6] D.-C. Kim, T.-H. Lee, M.-H. Choi, and Y.-H. Ha, "Color correction for projected image on colored screen based on a camera," in *Proc. SPIE Color Imaging XVI: Displaying, Processing, Hardcopy and Applications*, vol. 7866, pp. 786606–786606-8, 2011.

[7] D. Wang, I. Sato, T. Okabe, and Y. Sato, "Radiometric compensation in a projector-camera system based on the properties of human vision system," in *Proc. IEEE Int. Conf. Computer Vision and Pattern Recognition*, vol. 3, pp. 100–107, 2005.

[8] A. Majumder and R. Stevens, "Perceptual photometric seamlessness in projection-based tiled displays," *ACM Trans. Graphics*, vol. 24, pp. 118–139, 2005.

[9] M. Ashdown, T. Okabe, I. Sato, and Y. Sato, "Robust content-dependent photometric projector compensation," in *Proc. IEEE Conf. Computer Vision and Pattern Recognition Workshop*, pp. 17–22, 2006.

[10] O. Bimber, D. Iwai, G. Wetzstein, and A. Grundhöfer, "The visual computing of projector-camera systems," *Computer Graphics Forum*, vol. 27, no. 8, pp. 2219–2245, Dec. 2008.

[11] W. Zou and H. Xu, "Colorimetric color reproduction framework for screen relaxation of projection display," *Displays*, vol. 32, pp. 313–319, Dec. 2011.

[12] B. Zhu, L. Xie, T. Yang, Q. Wang, and Y. Zheng, "A novel radiometric projector compensation algorithm based on Lambertian reflection model," in *Proc. SPIE MIPPR: Pattern Recognition and Computer Vision*, vol. 8004, pp.1–5, 2011.

[13] T.-H. Huang, C.-T. Kao, and H. H. Chen, "Quality enhancement of procam system by radiometric compensation," in *Proc. IEEE 14th Int. Workshop Multimedia Signal Processing*, pp. 192–197, 2012.

[14] A. Gilchrist, C. Kossyfidis, F. Bonato, T. Agostini, J. Cataliotti, X. Li, B. Spehar, V. Annan, and E. Economou, "An anchoring theory of lightness perception," *Psychological Review*, vol. 106, pp. 795–834, 1999.

[15] T. Smith and J. Guild, "The C.I.E. colorimetric standards and their use," *Trans. Optical Soc.*, vol. 33, no. 3, pp. 73–134, Apr. 1932.

[16] N. Moroney, M.D. Fairchild, R.W.G. Hunt, C.J. Li, M.R. Luo, and T. Newman, "The CIECAM02 color appearance model," in *Proc. IS&T/SID 10th Color Imaging Conf.*, pp. 23–27, 2002.

[17] Wikimedia Foundation. (2013, May 7). *Specular highlight* [Online]. Available: http://en.wikipedia.org/wiki/Specular_highlight.

[18] Fractal coding and analysis group. (2009). *Repository* [Online]. Available: http://links.uwaterloo.ca/Repository.html.

[19] Kodak Lossless True Color Image Suite. (1999, Nov 15). *True Color Kodak Images* [Online]. Available: http://r0k.us/graphics/kodak/.

[20] The USC-SIPI Image Database. *SIPI Image Database* [Online]. Available: http://sipi.usc.edu/database/.

[21] Wikimedia Foundation. (2012, Dec 5). *Analysis of variance* [Online]. Available: http://en.wikipedia.org/wiki/Analysis_of_variance.

[22] Akiyoshi Kitaoka. (2011, Nov. 21). *Illusory color crosses* [Online]. Available: http://www.psy.ritsumei.ac.jp/~akitaoka/color14e.html.

[23] H. Park, M.-H. Lee, B.-K. Seo, J.-I. Park, M.-S. Jeong, T.-S. Park, Y. Lee, and S.-R. Kim, "Simultaneous geometric and radiometric adaptation to dynamic surfaces with a mobile projector-camera system," *IEEE Trans. Circuits Syst. Video Technol.*, vol. 18, no. 1, pp. 110–115, Jan. 2008.

[24] M. Ramasubramanian, S. N. Pattanaik, and D. P. Greenberg, "A perceptually based physical error metric for realistic image synthesis," *in Proc. the 26th annual conf. Computer graphics and interactive techniques*, pp. 73–82, 1999.

[25] S. N. Pattanaik, J. A. Ferwerda, M. D. Fairchild, and D. P. Greenberg, "A multiscale model of adaptation and spatial vision for realistic image display," in *Proc. the 25th annual conf. Computer graphics and interactive techniques*, pp. 287–298, 1998.

[26] J. A. Ferwerda, S. N. Pattanaik, P. Shirley, and D. P. Greenberg, "A model of visual masking for computer graphics," in *Proc. the 24th annual conf. Computer Graphics and Interactive Techniques*, pp. 143–152, 1997.

[27] M. D. Fairchild, M. R. Luo, and R. W. G. Hunt, "A revision of CIECAM97s for practical applications," *Color Research and Application*, vol. 25, no. 4, pp. 260–266, Aug. 2000.

[28] R. W. G. Hunt and M. R. Pointer, "A colour-appearance transform for the 1931 standard colorimetric observer," *Color Research and Application* vol. 10, no. 3, pp. 165–179, Aug. 1985.

[29] L. Michaelis and M. L. Menten, "Die Kinetik der Invertinwerkung," *Biochemische Zeitschrift*, vol. 49, pp. 333–369. Feb. 1913.

[30] Wikimedia Foundation. (2014, Jan. 14). *Additive color* [Online]. http://en.wikipedia.org/wiki/Additive_color.

[31] C. Li, M. R. Luo, R. R. Hunt, N. Moroney, M.D. Fairchild, and T. Newman, "The performance of CIECAM02," in *Proc. IS&T/SID 10th Color Imaging Conf.*, pp. 28–32, Scottsdale, AZ, Nov. 2002.

[32] T.-C. Wang, T.-H. Huang, and H. H. Chen. "Radiometric compensation for procam system based on anchoring theory." *IEEE. Int. Conf. Image Process*., pp. 103-107, Sept. 2013.

[33] P. Bodrogi and T. Q. Khan, (2012). Illumination, color and imaging: evaluation and optimization of visual displays. John Wiley & Sons, pp. 2–3.

[34] A. Grundhofer, "Practical non-linear photometric projector compensation." in *Proc. the IEEE Conf. Computer Vision and Pattern Recognition Workshops*, 2013.

[35] PetPixel. (2012, Nov. 17). *The camera versus the human eye* [Online]. http://petapixel.com/2012/11/17/the-camera-versus-the-human-eye/.

[36] K. Fujii, M. D. Grossberg, and S. K. Nayar, "A projector-camera system with real-time photometric adaptation for dynamic environments." in *Proc. IEEE Conf. Computer Vision and Pattern Recognition*, vol.1, pp. 814–821, 2005.

[37] M. A. Webster, J. A. Wilson, "Interactions between chromatic adaptation and contrast adaptation in color appearance," *Vision Research*, vol. 40, no. 28, pp. 3801–3816, 2000.

[38] Wikimedia Foundation. (2014, Jan. 14). *Student's t-test* [Online]. https://en.wikipedia.org/wiki/Student%27s_t-test.

[39] T.-H Huang, T.-C Wang, K.-T Shih, and H. H. Chen, "Perceptual radiometric compensation system adaptable to a projector-camera system," U.S. Patent 20150085162, Mar. 26, 2015.

Tai-Hsiang Huang received his M.S. degree in Electrical Engineering from National Taiwan University in 2008. He is currently working toward the Ph.D. degree in the Graduate Institute of Communication Engineering, National Taiwan University. His research interests are in the area of perceptual based image and video processing.

Ting-Chun Wang received the B.S. degree in electrical engineering from National Taiwan University, Taipei, Taiwan, in 2012. His research interests are in the area of multimedia information retrieval and analysis and signal processing.

Homer H. Chen (S'83–M'86–SM'01–F'03) received the Ph.D. degree in electrical and computer engineering from the University of Illinois at Urbana-Champaign.

Since August 2003, he has been with the College of Electrical Engineering and Computer Science, National Taiwan University, Taipei, Taiwan, where he is Irving T. Ho Chair Professor. Prior to that, he held various R&D management and engineering positions with U.S. companies over a period of 17 years, including AT&T Bell Labs, Rockwell Science Center, iVast, and Digital Island (acquired by Cable & Wireless). He was a U.S. delegate for ISO and ITU standards committees and contributed to the development of many new interactive multimedia technologies that are now part of the MPEG-4 and JPEG-2000 standards. His professional interests lie in the broad area of multimedia signal processing and communications.

Dr. Chen was an Associate Editor of the IEEE Transactions on Circuits and Systems for Video Technology from 2004 to 2010, the IEEE Transactions on Image Processing from 1992 to 1994, and Pattern Recognition from 1989 to 1999. He served as a Guest Editor for the IEEE Transactions on Circuits and systems for video Technology in 1999, the IEEE Transactions on Multimedia in 2011, IEEE Journal of Selected Topics in Signal Processing in 2014, and the Springer Multimedia Applications and Tools in 2015. Currently he is on the Fourier Award Committee and the Fellow Reference Committee of the IEEE Signal Processing Society.